Eur. Phys. J. B **20**, 451–467 (2001)

THE EUROPEAN PHYSICAL JOURNAL B

EDP Sciences

Coherent control of the self-trapping transition

M. Holthaus[1,a] and S. Stenholm[2]

[1] Carl von Ossietzky Universität, Fachbereich Physik, 26111 Oldenburg, Germany
[2] Physics Department, Royal Institute of Technology, Lindstedtsvägen 24, 10044 Stockholm, Sweden

Received 5 November 2000 and Received in final form 16 February 2001

Abstract. We discuss the dynamics of two weakly coupled Bose-Einstein condensates in a double-well potential, contrasting the mean-field picture to the exact N-particle evolution. On the mean-field level, a self-trapping transition occurs when the scaled interaction strength exceeds a critical value; this transition essentially persists in small condensates comprising about 1000 atoms. When the double-well is modulated periodically in time, Floquet-type solutions to the nonlinear Schrödinger equation take over the role of the stationary mean-field states. These nonlinear Floquet states can be classified as "unbalanced" or "balanced", depending on whether or not they entail long-time confinement of most particles to one well. Since the emergence of unbalanced Floquet states depends on the amplitude and frequency of the modulating force, we predict that the onset of self-trapping can efficiently be controlled by varying these parameters. This prediction is verified numerically by both mean-field and N-particle calculations.

PACS. 03.75.Fi Phase coherent atomic ensembles; quantum condensation phenomena – 05.30.Jp Boson systems – 32.80.Pj Optical cooling of atoms; trapping

1 Introduction

When dealing with quantum mechanical many-particle systems, the mean-field approximation is an indispensable tool. Yet, this approximation introduces a nonlinearity, and in general it is not obvious whether phenomena typically associated with nonlinear equations, such as bifurcations in the spectrum of the stationary states, actually find their counterpart in the true many-body dynamics, or whether they are merely an artifact of the approximation. Simple models which can be solved exactly both on the mean-field level and on the level of the many-body Schrödinger equation, and thus lend themselves to a test of the mean-field picture, are therefore of particular importance.

In this paper we present an extensive study of such a model, describing two weakly coupled Bose-Einstein condensates at zero temperature under the influence of external time-periodic forcing. It had been pointed out already before the experimental realization of dilute Bose-Einstein condensates with alkali atoms [1] that a weak tunnelling contact between two such condensates should give rise to a Josephson-like oscillatory exchange of atoms [2,3]; after the feasibility of creating such weak tunnelling links had been demonstrated in the laboratory [4], this neutral-particle analogue of the Josephson effect has become the subject of several theoretical studies [5–9]. We take up the two-mode model for coupled condensates put forward by Milburn *et al.* [5], and extend it by adding a periodic force. After stating the algebraic properties of this model in Section 2, and estimating the magnitude of the crucial dimensionless parameter α that embodies the strength of the interaction among the condensed particles, Section 3 provides a detailed comparison of mean-field and many-body dynamics in the absence of the driving force. On the mean-field level, the model then shows a "self-trapping transition" [5,6,8] which had originally been encountered in the context of the motion of a polaron on a dimer by Kenkre and Campbell [10]; we investigate why, how, and to which extent this mean-field transition reflects an actual feature of the underlying many-body model. This discussion sets the stage for Section 4, where we show that the self-trapping transition can be controlled by the periodic force: If such a force is acting on the system, the self-trapping transition still occurs, but for a value of the scaled interaction strength α which now depends on strength and frequency of the drive. This novel effect might find applications for measuring the s-wave scattering length of condensed atoms, or for determining the number of atoms in comparatively small condensates. The new theoretical concept which leads to this discovery, and which allows us to discuss the dynamics of periodically forced, coupled condensates in close analogy to the undriven case, is the notion of Floquet states for the nonlinear Schrödinger equation [11]. These states constitute a generalization of the Floquet states known from quantum systems governed by a time-periodic Hamiltonian [12,13] to nonlinear mean-field equations of the Gross-Pitaevskii type. Essentially, the "nonlinear" Floquet states take over

[a] e-mail: holthaus@marvin.physik.uni-oldenburg.de

the role played in the absence of the force by stationary mean-field solutions; since they incorporate this force in a non-perturbative manner, they provide an efficient access to the intricate time evolution of the driven many-body system. In particular, the dependence of the Floquet states on strength and frequency of the periodic drive holds the key for understanding the systematics of coherent control of the self-trapping transition. Besides the "active" view of steering that transition through parameter space by suitably adjusting the force, our results also lend strong support to a "passive" interpretation: The periodic force effectively renormalizes the strength of the interaction among the Bose-Einstein-condensed particles. This viewpoint will be substantiated in the concluding Section 5.

2 The model

Consider a Bose-Einstein condensate consisting of N atoms at zero temperature and confined by a symmetric double-well potential $V(\mathbf{r})$, realized experimentally by a combination of magnetic and optical forces [4]. Assume further that this potential is modulated periodically in time with angular frequency ω, such that the Gross-Pitaevskii mean-field equation for the macroscopic wave function $\Psi(\mathbf{r},t)$ adopts the form

$$\mathrm{i}\hbar\frac{\partial}{\partial t}\Psi(\mathbf{r},t) = \left(-\frac{\hbar^2}{2m}\Delta + V(\mathbf{r}) + \mathbf{F}\cdot\mathbf{r}\sin(\omega t) + Ng|\Psi(\mathbf{r},t)|^2\right)\Psi(\mathbf{r},t), \tag{1}$$

where

$$g = \frac{4\pi a_{\mathrm{sc}}\hbar^2}{m} \tag{2}$$

quantifies the interaction strength, with a_{sc} and m denoting the s-wave scattering length and the mass of the condensed atomic species, respectively, and $\Psi(\mathbf{r},t)$ is normalized to unity, $\int \mathrm{d}^3r\,|\Psi(\mathbf{r},t)|^2 = 1$. We stipulate that the modulating force $\mathbf{F}$ be directed along the line connecting the two minima of the potential, so that the bottoms of the two wells move in phase opposition: The left one goes down when the right one goes up, and *vice versa*. Let now $u_1(\mathbf{r})$ and $u_2(\mathbf{r})$ be the lowest Wannier-like single-particle orbitals localized in the individual wells. Their even and odd linear combinations

$$\begin{aligned} u_+(\mathbf{r}) &= \frac{1}{\sqrt{2}}\left[u_1(\mathbf{r}) + u_2(\mathbf{r})\right] \\ u_-(\mathbf{r}) &= \frac{1}{\sqrt{2}}\left[u_1(\mathbf{r}) - u_2(\mathbf{r})\right] \end{aligned} \tag{3}$$

are approximate eigenfunctions of the single-particle Hamiltonian $H_0 = -\frac{\hbar^2}{2m}\Delta + V(\mathbf{r})$:

$$H_0\,u_\pm(\mathbf{r}) = E_\pm u_\pm(\mathbf{r}), \tag{4}$$

with $E_+ < E_-$. If the dynamics of the driven Bose-Einstein condensate remains essentially restricted to this doublet of states, one can resort to the ansatz [5]

$$\Psi(\mathbf{r},t) = \exp(-\mathrm{i}E_0t/\hbar)\left[c_1(t)u_1(\mathbf{r}) + c_2(t)u_2(\mathbf{r})\right], \tag{5}$$

where $E_0 = \frac{1}{2}(E_+ + E_-)$. The squares $|c_1(t)|^2$ and $|c_2(t)|^2 = 1 - |c_1(t)|^2$, multiplied by the total particle number N, then give the expectation values for the numbers of particles found in the first and second well. The equations of motion for the amplitudes $c_1(t)$ and $c_2(t)$ follow in the usual way by inserting the ansatz (5) into the Gross-Pitaevskii equation (1) and taking the scalar product with $u_1(\mathbf{r})$ and $u_2(\mathbf{r})$, respectively. We introduce the tunnelling splitting

$$\hbar\Omega = E_- - E_+ \tag{6}$$

and the on-site interaction energy per particle

$$\hbar\kappa = \frac{g}{2}\int \mathrm{d}^3r\,|u_1(\mathbf{r})|^4, \tag{7}$$

and employ the position matrix elements

$$\begin{aligned} \int \mathrm{d}^3r\,u_1^*(\mathbf{r})\,\mathbf{r}\,u_1(\mathbf{r}) &= \mathbf{d} \\ \int \mathrm{d}^3r\,u_2^*(\mathbf{r})\,\mathbf{r}\,u_2(\mathbf{r}) &= -\mathbf{d}, \end{aligned} \tag{8}$$

where the origin of the coordinate system is located in the center of the barrier, to define the Rabi frequency

$$\mu = \frac{Fd}{\hbar}\cdot \tag{9}$$

Since $\mathbf{F}$ is assumed to be parallel to $\mathbf{d}$, only the absolute magnitudes of these vectors enter here; $2d$ is the distance between the minima of the two wells. Moreover, we neglect the overlap of the localized orbitals, $u_1(\mathbf{r})u_2(\mathbf{r}) \approx 0$. This approximation implies that the condensates situated in the individual wells are merely weakly coupled; a more general treatment not subject to this restriction, but without the periodic drive, has been given by Spekkens and Sipe [14]. One thus arrives at the system

$$\begin{aligned} \mathrm{i}\frac{\mathrm{d}}{\mathrm{d}t}c_1(t) &= -\frac{\Omega}{2}\,c_2(t) + 2N\kappa\,|c_1(t)|^2\,c_1(t) + \mu\sin(\omega t)\,c_1(t) \\ \mathrm{i}\frac{\mathrm{d}}{\mathrm{d}t}c_2(t) &= -\frac{\Omega}{2}\,c_1(t) + 2N\kappa\,|c_2(t)|^2\,c_2(t) - \mu\sin(\omega t)\,c_2(t). \end{aligned} \tag{10}$$

Using the dimensionless time variable

$$\tau = \Omega t, \tag{11}$$

these equations become

$$\begin{aligned} \mathrm{i}\,\dot{c_1} &= -\frac{1}{2}\,c_2 + 2\frac{N\kappa}{\Omega}\,|c_1|^2\,c_1 + \frac{\mu}{\Omega}\sin\Big(\frac{\omega}{\Omega}\tau\Big)\,c_1 \\ \mathrm{i}\,\dot{c_2} &= -\frac{1}{2}\,c_1 + 2\frac{N\kappa}{\Omega}\,|c_2|^2\,c_2 - \frac{\mu}{\Omega}\sin\Big(\frac{\omega}{\Omega}\tau\Big)\,c_2, \end{aligned} \tag{12}$$

where here and henceforth the dot denotes differentiation with respect to τ, and the dependence of the on-site amplitudes c_1, c_2 on τ is suppressed.

The system (12) contains three dimensionless parameters: The ratio $N\kappa/\Omega$ of the N-particle interaction energy to the single-particle tunnelling splitting (6), the ratio μ/Ω of the Rabi frequency (9) to the tunnelling frequency Ω, and the ratio ω/Ω of the driving frequency ω to the tunnelling frequency. For estimating the relevant orders of magnitude, it suffices to consider a one-dimensional double-well potential $V(x)$ with minima at $x = \pm d$, so that the tunnelling splitting is given by [15,16]

$$\hbar\Omega = \frac{2\hbar^2}{m} u_1(0) u_1'(0). \tag{13}$$

Assuming the two wells to be about harmonic, one may approximate $u_1(x)$ and $u_2(x)$ by harmonic oscillator functions,

$$u_{1,2}(x) = \frac{1}{(2\pi\ell^2)^{1/4}} \exp\left(-\frac{(x \pm d)^2}{4\ell^2}\right), \tag{14}$$

where the oscillator length ℓ is related to the frequency ω_0 of oscillations within one well by $\ell = \sqrt{\hbar/(2m\omega_0)}$. Then equation (13) yields

$$\hbar\Omega = \hbar\omega_0 \sqrt{\frac{2}{\pi}} \frac{d}{\ell} \exp\left(-\frac{d^2}{2\ell^2}\right), \tag{15}$$

indicating that the tunnelling frequency differs from the oscillation frequency by a factor which is determined solely by the ratio d/ℓ. For instance, if $d/\ell = 2$, meaning that the distance between the two minima is four times the oscillator length, one obtains $\hbar\Omega \approx 0.22\,\hbar\omega_0$. Taking comparatively shallow wells with $\omega_0 = 100\ \mathrm{s}^{-1}$, say, which corresponds to $\ell \approx 3.7\ \mu$m for ^{23}Na atoms, one thus ends up with $\Omega \approx 22\ \mathrm{s}^{-1}$.

Next, assuming the bottoms of the two wells to be roughly isotropic, the three-dimensional analogues of the functions (14) lead to

$$\int \mathrm{d}^3 r\, |u_1(\mathbf{r})|^4 = \frac{1}{8\pi^{3/2}\ell^3}, \tag{16}$$

implying

$$\hbar\kappa = \frac{\hbar^2}{2m\ell^2} \frac{a_{\mathrm{sc}}}{2\sqrt{\pi}\,\ell}\,. \tag{17}$$

Inserting $a_{\mathrm{sc}} = 2.75$ nm for ^{23}Na atoms [17], together with the same ℓ as above, one finds $\kappa \approx 0.021\ \mathrm{s}^{-1}$, or $\kappa/\Omega \approx 0.97 \times 10^{-3}$. Hence, under quite realistic conditions the interaction parameter $N\kappa/\Omega$ is on the order of unity for $N \approx 1000$ particles.

The two-mode approximation (5) can be expected to hold as long as the many-body interaction energy remains small compared to the ground-state energies of the two wells [5]. This gives the condition $N\hbar\kappa \ll \hbar\omega_0$, or

$$N \ll 2\sqrt{\pi}\,\ell/a_{\mathrm{sc}} \tag{18}$$

on the particle number N; with the above parameters, this amounts to $N \ll 4800$. Thus, the two-mode approximation in the form (5) is valid only for quite small condensates. In addition, the Rabi frequency should remain small compared to the oscillator frequency, $\mu \ll \omega_0$. Since, according to the estimate (15), the tunnelling frequency Ω will typically figure as a few tenths of ω_0, the parameter μ/Ω can be as high as 10 for admissible forces, while the driving frequency ω should be on the order of Ω at most. It should also be noted that the assumption of isotropic traps underlying these order-of-magnitude estimates has to be abandoned for traps with large aspect ratios, but the estimates can easily be adapted to such cases.

Besides the basic system (12), there are two other representations of the equations of motion that will be found useful. Defining the quantities [5]

$$\begin{aligned} K_x &= \frac{1}{2}\left(c_1^* c_2 + c_1 c_2^*\right) \\ K_y &= -\frac{\mathrm{i}}{2}\left(c_1^* c_2 - c_1 c_2^*\right) \\ K_z &= \frac{1}{2}\left(|c_1|^2 - |c_2|^2\right), \end{aligned} \tag{19}$$

the significance of which will become obvious soon, one gets

$$\begin{aligned} \dot{K}_x &= -4\,\frac{N\kappa}{\Omega} K_y K_z - 2\,\frac{\mu}{\Omega} \sin\Big(\frac{\omega}{\Omega}\tau\Big) K_y \\ \dot{K}_y &= +4\,\frac{N\kappa}{\Omega} K_z K_x + 2\,\frac{\mu}{\Omega} \sin\Big(\frac{\omega}{\Omega}\tau\Big) K_x + K_z \\ \dot{K}_z &= -K_y. \end{aligned} \tag{20}$$

On the other hand, decomposing the amplitudes into absolute magnitudes and phase factors according to $c_1 = |c_1| \exp(\mathrm{i}\vartheta_1)$, $c_2 = |c_2| \exp(\mathrm{i}\vartheta_2)$ [6,8], and invoking the population imbalance

$$p = |c_1|^2 - |c_2|^2 \tag{21}$$

and the relative phase

$$\varphi = \vartheta_2 - \vartheta_1, \tag{22}$$

a short calculation results in

$$\begin{aligned} \dot{p} &= -\sqrt{1-p^2}\,\sin(\varphi) \\ \dot{\varphi} &= 2\frac{N\kappa}{\Omega} p + \frac{p}{\sqrt{1-p^2}}\cos(\varphi) + 2\frac{\mu}{\Omega}\sin\Big(\frac{\omega}{\Omega}\tau\Big). \end{aligned} \tag{23}$$

These latter equations have an appealing Hamiltonian form: Introducing

$$H_{\mathrm{nrp}} = \frac{N\kappa}{\Omega} p^2 - \sqrt{1-p^2}\,\cos(\varphi) + 2\frac{\mu}{\Omega} p \sin\Big(\frac{\omega}{\Omega}\tau\Big), \tag{24}$$

one has

$$\begin{aligned} \dot{p} &= -\frac{\partial H_{\mathrm{nrp}}}{\partial \varphi} \\ \dot{\varphi} &= \frac{\partial H_{\mathrm{nrp}}}{\partial p}\,. \end{aligned} \tag{25}$$

In this representation, the population imbalance p corresponds to the momentum of a periodically forced nonrigid pendulum, that is, a pendulum with a length depending on p [6], with φ denoting its angle of displacement, and $N\kappa/\Omega$ playing the role of its inverse mass.

The equivalent equations of motion (12, 20, 23) all stem from the mean-field Hamiltonian

$$H_{\rm mf} = -\frac{\hbar\Omega}{2}\left(c_1 c_2^* + c_1^* c_2\right) + N\hbar\kappa\left(|c_1|^4 + |c_2|^4\right) + \hbar\mu\sin(\omega t)\left(|c_1|^2 - |c_2|^2\right), \tag{26}$$

which is what remains within the two-mode approximation (5) from the original Gross-Pitaevskii Hamiltonian underlying equation (1). It is now of major interest that if one adheres to the two-mode approximation, the mean-field approximation can be abandoned: If there are N identical Bosons on two sites, the number of particles found on either of these sites can take on any integer between and including 0 and N. Hence, the dimension of the N-particle Hilbert space is merely $N+1$, easily accessible to numerical analysis even for quite substantial values of N. Thus, replacing the c-number amplitudes c_1, c_2, and their complex conjugates, by Bose operators b_1, b_2 which annihilate a particle at the respective site, and their adjoint creation operators, subject to the commutation rules

$$[b_k, b_l^\dagger] = \delta_{kl}, \tag{27}$$

the N-particle counterpart of the mean-field Hamiltonian (26) takes the form

$$H_{N\rm p} = -\frac{\hbar\Omega}{2}\left(b_1 b_2^\dagger + b_1^\dagger b_2\right) + \hbar\kappa\left(b_1^\dagger b_1^\dagger b_1 b_1 + b_2^\dagger b_2^\dagger b_2 b_2\right) + \hbar\mu\sin(\omega t)\left(b_1^\dagger b_1 - b_2^\dagger b_2\right). \tag{28}$$

Adapting then the definitions (19) and introducing the operators [5]

$$J_x = \frac{1}{2}\left(b_1^\dagger b_2 + b_1 b_2^\dagger\right)$$
$$J_y = -\frac{\mathrm{i}}{2}\left(b_1^\dagger b_2 - b_1 b_2^\dagger\right)$$
$$J_z = \frac{1}{2}\left(b_1^\dagger b_1 - b_2^\dagger b_2\right), \tag{29}$$

one finds that these expressions obey the familiar SU(2) commutation relations

$$[J_k, J_l] = \mathrm{i}\varepsilon_{klm} J_m, \tag{30}$$

that is, they represent the three components of an angular momentum-type operator. (It is, of course, this fact which first motivates one to consider the operators (29) and then, backwards, their classical analogues (19); rather than the other way round.) Calculating the Casimir invariant

$$J_x^2 + J_y^2 + J_z^2 = \frac{N}{2}\left(\frac{N}{2} + 1\right), \tag{31}$$

one sees that this angular momentum is of magnitude $N/2$, so that its $2(N/2)+1 = N+1$ states match precisely the $N+1$ basis states of the N-particle Hilbert space.

Expressed in terms of these angular momentum operators, the Hamiltonian (28) reads

$$H_{N\rm p} = -\hbar\Omega J_x + 2\hbar\kappa J_z^2 + 2\hbar\mu\sin(\omega t) J_z + \frac{1}{2}\hbar\kappa N(N-2), \tag{32}$$

and the Heisenberg equations of motion become

$$\dot{J}_x = -2\,\frac{\kappa}{\Omega}(J_y J_z + J_z J_y) - 2\,\frac{\mu}{\Omega}\sin\Big(\frac{\omega}{\Omega}\tau\Big)\, J_y$$
$$\dot{J}_y = +2\,\frac{\kappa}{\Omega}(J_z J_x + J_x J_z) + 2\,\frac{\mu}{\Omega}\sin\Big(\frac{\omega}{\Omega}\tau\Big)\, J_x + J_z$$
$$\dot{J}_z = -J_y. \tag{33}$$

Comparing these equations for the N-particle system to their mean-field counterparts (20), one sees that the mean-field approximation formally consists (apart from writing NK_k for J_k) merely in the substitution

$$\frac{1}{2}(J_y J_z + J_z J_y) \longrightarrow N^2 K_y K_z, \tag{34}$$

and the analogous substitution in the second equation (33); but it is not obvious at all to which extent these replacements of non-commuting operators by c-numbers affect or even falsify the dynamics [5,18]. This matter will be investigated further in the following two sections.

For juxtaposing the nonlinear mean-field dynamics to the exact evolution of the quantum system, one has to know the N-particle counterpart of a given mean-field state $\left(c_1, c_2 = \sqrt{1-c_1^2}\,\exp(\mathrm{i}\varphi)\right)$, where the amplitude c_1 may be chosen real. This pair contains the information that there are, on the average, Nc_1^2 atoms in the first well, and that the relative phase between the condensate in the first and in the second well is φ. In a fully quantum mechanical setting, when one is in possession of the information that each individual atom has the probability $c_1^2 \equiv \cos^2(\vartheta/2)$ of staying in the first well, one still has to deal with the coherent superposition of the possibilities that there actually is any number n_1 of particles between 0 and N in the first well, while each of the $n_2 = N - n_1$ remaining particles in the second well contributes a relative phase φ; here the assumption of dealing with phase-coherent Bose-Einstein condensates enters. Hence, writing the Fock states with n_1 atoms in the first and n_2 atoms in the second well as $|n_1, n_2\rangle$, and recalling the properties of the Binomial probability distribution, the N-particle states corresponding to the mean-field states $(c_1, c_2) = (\cos(\vartheta/2)\,,\, \sin(\vartheta/2)\exp(\mathrm{i}\varphi))$ evidently are

$$|\vartheta, \varphi\rangle = \sum_{n_1=0}^{N} \binom{N}{n_1}^{1/2} \cos^{n_1}(\vartheta/2)\, \sin^{n_2}(\vartheta/2)\, \mathrm{e}^{\mathrm{i}n_2\varphi}\, |n_1, n_2\rangle. \tag{35}$$

These "atomic" coherent states had previously been studied in detail in reference [19] and, in particular, in reference [20], where also their relationship to the standard

coherent states has been investigated; they have also been considered by Milburn *et al.* [5] and Raghavan *et al.* [18] in a discussion of non-driven condensate tunnelling. Interestingly,

$$\begin{aligned}\langle\vartheta,\varphi|J_x|\vartheta,\varphi\rangle &= \frac{N}{2}\sin\vartheta\cos\varphi\\ \langle\vartheta,\varphi|J_y|\vartheta,\varphi\rangle &= \frac{N}{2}\sin\vartheta\sin\varphi\\ \langle\vartheta,\varphi|J_z|\vartheta,\varphi\rangle &= \frac{N}{2}\cos\vartheta,\end{aligned} \tag{36}$$

so that a coherent state (35) may conveniently be visualized by the tip of a vector moving on a unit sphere.

3 The self-trapping transition

We will now investigate the validity of the mean-field approximation in the absence of the driving force, *i.e.*, for $\mu/\Omega = 0$ [5,18], so that the only relevant parameter is the scaled interaction energy

$$\alpha \equiv \frac{N\kappa}{\Omega}\,. \tag{37}$$

To begin with, we find the stationary states of the nonlinear Schrödinger equation [21], that is, solutions of the form

$$c_{1,2}(\tau) = \psi_{1,2}\exp(-\mathrm{i}\nu\tau) \tag{38}$$

with real (dimensionless) frequency ν. These states follow from the nonlinear eigenvalue problem

$$\begin{aligned}\nu\psi_1 &= -\frac{1}{2}\psi_2 + 2\alpha|\psi_1|^2\psi_1\\ \nu\psi_2 &= -\frac{1}{2}\psi_1 + 2\alpha|\psi_2|^2\psi_2,\end{aligned} \tag{39}$$

or

$$\begin{aligned}\nu|\psi_1|^2 &= -\frac{1}{2}\psi_1^*\psi_2 + 2\alpha|\psi_1|^4\\ \nu|\psi_2|^2 &= -\frac{1}{2}\psi_1\psi_2^* + 2\alpha|\psi_2|^4.\end{aligned} \tag{40}$$

Since ψ_1, ψ_2 are determined only up to an overall phase factor we may choose ψ_1 as real, so that, by virtue of equations (40), also ψ_2 must be real. Subtracting these two equations, and using $\psi_1^2 + \psi_2^2 = 1$, one arrives at

$$\nu\left(2\psi_1^2 - 1\right) = 2\alpha\left(2\psi_1^2 - 1\right), \tag{41}$$

which leaves us with the following alternative:

(i) Either we have $2\psi_1^2 - 1 = 0$, giving "balanced" states with equal population of both wells,

$$\begin{aligned}\psi_1 &= \frac{1}{\sqrt{2}}\\ \psi_2 &= \pm\frac{1}{\sqrt{2}}\,.\end{aligned} \tag{42}$$

The frequencies of these two solutions are

$$\nu_\pm = \alpha \mp \frac{1}{2}, \tag{43}$$

and the corresponding energies per particle, measured in multiples of the single-particle tunnelling energy, turn out to be

$$\frac{E_\pm/N}{\hbar\Omega} = \frac{\alpha}{2} \mp \frac{1}{2}\,. \tag{44}$$

(ii) Or we have $\nu = 2\alpha$ in equation (41), in which case one finds

$$\psi_1\psi_2 = -\frac{1}{4\alpha} \tag{45}$$

by adding the two equations (40). This means that the two amplitudes must have the opposite sign if α, and hence κ, is positive; according to equations (2) and (7), this occurs when the scattering length a_{sc} is positive, so that the interaction among the atoms is repulsive. On the other hand, for negative scattering length and attractive interaction, as is the case for condensates of ^{7}Li [22], both amplitudes must have the same sign. Squaring equation (45) then gives

$$\psi_1^2\left(1 - \psi_1^2\right) = \frac{1}{(4\alpha)^2}, \tag{46}$$

leading immediately to

$$\begin{aligned}\psi_1 &= \frac{1}{\sqrt{2}}\left(1 + \sqrt{1 - \frac{1}{4\alpha^2}}\right)^{1/2}\\ \psi_2 &= -\frac{\mathrm{sign}(\alpha)}{\sqrt{2}}\left(1 - \sqrt{1 - \frac{1}{4\alpha^2}}\right)^{1/2};\end{aligned} \tag{47}$$

a further solution is obtained by interchanging the indices 1 and 2, thereby swapping the populations in the two wells. Whereas the previous balanced solutions (42) exist for any α, these latter solutions (47) with "unbalanced" distribution of atoms over the wells exist only for sufficiently strong interaction, $|\alpha| = N|\kappa|/\Omega \geq 1/2$; their energy is

$$\frac{E/N}{\hbar\Omega} = \alpha + \frac{1}{8\alpha}\,. \tag{48}$$

For $\alpha > 0$, the solution (47) and its population-swapped counterpart bifurcate at $\alpha = 1/2$ from the "upper" solution (42) (meaning the solution with a relative phase of π between both amplitudes, which gives the higher energy (44)), whereas for $\alpha < 0$ the unbalanced states bifurcate at $\alpha = -1/2$ from the solution with zero relative phase, corresponding to the lower energy (44). Standard linear stability analysis [21] reveals that the branch from which the unbalanced states bifurcate becomes unstable at the bifurcation point, whereas all other solutions are stable; the bifurcation therefore is

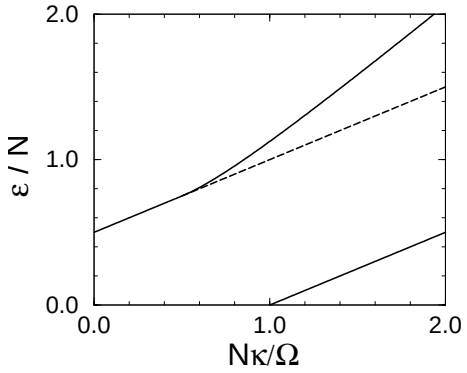

Fig. 1. Mean-field energies $\varepsilon = E/\hbar\Omega$ of the "balanced" states (42) and of the "unbalanced" states of the type (47), for repulsive interaction (positive κ). As indicated by the dashed line, the balanced state with the higher energy (44) becomes linearly unstable when the unbalanced states bifurcate off, whereas all other states are linearly stable.

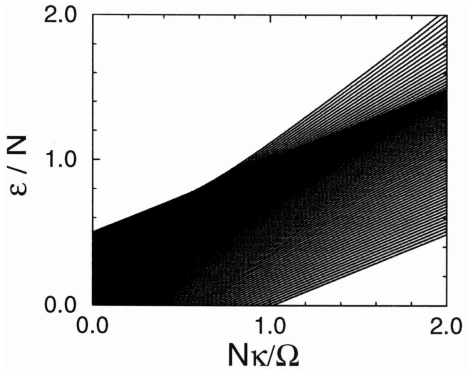

Fig. 2. Exact energy eigenvalues $\varepsilon_n = E_n/\hbar\Omega$ of the N-particle Hamiltonian (28) with $\mu/\Omega = 0$, for $N = 100$ Bose particles. Observe the striking resemblance of this figure to the mean-field energies displayed in Figure 1.

of the pitchfork type [23]. Figure 1 shows the energies (44) and (48) for positive α; stable states are indicated by solid and unstable states by dashed lines. The corresponding diagram for negative α is obtained by rotating the figure by 180 degrees around the origin. Thus, for repulsive interaction the mean-field ground state always features the same number of atoms in both wells, whereas for attractive interaction it becomes energetically favourable to collect more atoms in one of the wells when $|\alpha| > 1/2$.

The bifurcation depicted in Figure 1 reflects the nonlinearity of the mean-field eigenvalue problem (40). Considering the fact that eigenvalues of the linear Schrödinger operator describing the N-particle problem do not bifurcate, what is the meaning of this bifurcation for the exact quantum dynamics? Figure 2 shows the exact energy eigenvalues of the Hamiltonian (28) with $\mu/\Omega = 0$, for $N = 100$. There is a fairly strong resemblance of this figure to the previous one; the energies of the highest and lowest N-particle state closely follow those of the linearly stable mean-field states. Yet, for graphically resolving all

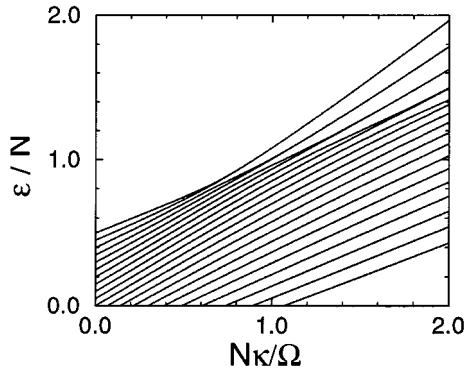

Fig. 3. Exact energy eigenvalues $\varepsilon_n = E_n/\hbar\Omega$ of the N-particle Hamiltonian (28) with $\mu/\Omega = 0$, for $N = 20$ Bose particles. Note that the linearly unstable mean-field eigenvalue in Figure 1, considered as a function of $\alpha = N\kappa/\Omega$, does not correspond to an individual eigenvalue, or pair of eigenvalues, of the N-particle problem.

details of the spectrum even $N = 100$ appears too large; the systematics become more clear in Figure 3, where N has been reduced to 20: There are essentially two groups of energy levels; those that still follow the low-α-pattern even for $\alpha > 1$, and those that "bend off", following the unbalanced mean-field states. These latter states become pairwise degenerate (roughly) when they cross the dashed line marked by the linearly unstable mean-field state in Figure 1. In terms of the angular momentum form (32) of the Hamiltonian, the first group of states is dominated by the operator J_x, that is, by well-to-well tunnelling, whereas the second group is dominated by J_z^2, that is, by the interaction among the particles. The pairwise degeneracy of these interaction-dominated states obviously is related to spontaneous symmetry breaking: If there is an unbalanced population, the majority of the atoms could be sitting in either the right or the left well. It is thus interesting to observe that when the interaction makes itself felt while increasing α, it does not affect all quantum states simultaneously but rather gradually, pair by pair. It also seems worth mentioning that the linearly stable mean-field states directly correspond to individual N-particle states, or pairs of such states, namely the states with the highest and lowest energy, but there is no such simple, continuous correspondence for the linearly unstable states when α is varied.

Resorting to the coherent states (35), the even balanced mean-field state (42) corresponds to the coherent state

$$|\pi/2, 0\rangle = \frac{1}{2^{N/2}} \sum_{n_1=0}^{N} \binom{N}{n_1}^{1/2} |n_1, n_2\rangle, \qquad (49)$$

and the odd balanced state (42) to

$$|\pi/2, \pi\rangle = \frac{1}{2^{N/2}} \sum_{n_1=0}^{N} \binom{N}{n_1}^{1/2} (-1)^{N-n_1} |n_1, n_2\rangle. \qquad (50)$$

The unbalanced mean-field state (47) and its swapped counterpart require more care, since the N-particle Hamiltonian (28) respects parity when $\mu/\Omega = 0$. Hence, all its energy eigenfunctions must be of the balanced type, describing modes with equal numbers of particles in both wells. Therefore, if we construct the coherent N-particle state (35) corresponding to the mean-field state (47), and the mirror image

$$\overline{|\vartheta,\varphi\rangle} = \sum_{n_1=0}^{N} \binom{N}{n_1}^{1/2} \cos^{n_1}(\vartheta/2)\, \sin^{n_2}(\vartheta/2)\, \mathrm{e}^{\mathrm{i}n_2\varphi}\, |n_2, n_1\rangle \tag{51}$$

for its counterpart, then these two coherent states do not approximate individual N-particle energy eigenstates, in contrast to the states (49) and (50). Instead, in order to reconcile the occurrence of unbalanced mean-field states with the necessity of perfectly balanced, exact N-particle eigenstates, one has to form the balanced linear combinations

$$|\Psi_\pm\rangle = \frac{1}{C}\left(|\vartheta,\varphi\rangle \pm \overline{|\vartheta,\varphi\rangle}\right), \tag{52}$$

where the constant C is to ensure normalization (note that $|\vartheta,\varphi\rangle$ and $\overline{|\vartheta,\varphi\rangle}$ are not necessarily orthogonal, although they tend to be so for large $|\alpha|$), and

$$\cos(\vartheta/2) = \frac{1}{\sqrt{2}}\left(1+\sqrt{1-\frac{1}{4\alpha^2}}\right)^{1/2}$$
$$\varphi = \begin{cases} \pi \text{ for } \alpha > 0 \\ 0 \text{ for } \alpha < 0 \end{cases}. \tag{53}$$

This procedure of getting "delocalized" eigenstates from "localized" partial solutions is analogous to the construction made in equation (3).

If α is positive and the interaction repulsive, as in the previous figures, one thus expects the state (49) to provide a fair approximation to the exact N-particle ground state $|u_0\rangle$; the highest N-particle state $|u_N\rangle$ should be well approximated by the state (50) as long as $\alpha < 1/2$. When $\alpha > 1/2$, the highest pair of almost degenerate N-particle states, $|u_N\rangle$ and $|u_{N-1}\rangle$, should almost coincide with the pair (52). This expectation is confirmed in Figure 4, which shows the squared projection of $|\pi/2, 0\rangle$ on $|u_0\rangle$ (inset), the squared projection of $|\pi/2, \pi\rangle$ on $|u_N\rangle$ (dashed curve), and the sum of the squared projections of the unbalanced coherent state $|\vartheta,\varphi\rangle$ with parameters (53) to $|u_N\rangle$ and $|u_{N-1}\rangle$. We avoid considering the individual projections, since this requires to numerically resolve the tiny difference between the almost degenerate energies of $|u_N\rangle$ and $|u_{N-1}\rangle$. However, for comparatively small N, such as $N = 20$ as in Figure 4, this resolution poses no problem, and we have checked that for $\alpha > 1$ the highest eigenstate $|u_N\rangle$ coincides almost exactly with the superposition $|\Psi_+\rangle$, while $|u_{N-1}\rangle$ is approximated to the same level of accuracy by $|\Psi_-\rangle$. Although the particle number N is merely 20 in Figure 4, the expected crossover

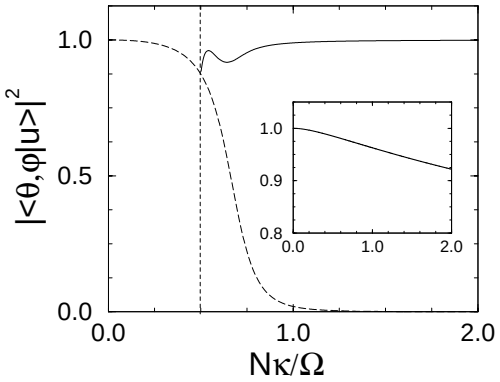

Fig. 4. Squared projection $|\langle\pi/2, 0|u_0\rangle|^2$ of the coherent state (49) to the exact N-particle ground state $|u_0\rangle$ (inset), and squared projection $|\langle\pi/2, \pi|u_N\rangle|^2$ of the coherent state (50) to the highest N-particle energy eigenstate $|u_N\rangle$ (main figure, dashed curve), together with the sum $|\langle\vartheta,\varphi|u_N\rangle|^2 + |\langle\vartheta,\varphi|u_{N-1}\rangle|^2$ of the squared projections of the coherent state (35) with parameters (53) to the highest two N-particle eigenstates. For $N\kappa/\Omega > 1$ each summand contributes almost exactly 0.5, indicating that the coherent state $|\vartheta,\varphi\rangle$ is an equal-weight superposition of the almost degenerate pair $|u_N\rangle$ and $|u_{N-1}\rangle$. The number of particles is $N = 20$.

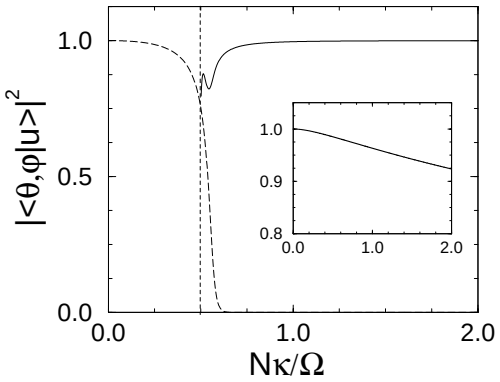

Fig. 5. As Figure 4, for $N = 100$. Note that at $N\kappa/\Omega = 0.5$ the drop of the dashed curve, representing the overlap $|\langle\pi/2, \pi|u_N\rangle|^2$, is already quite rapid.

is already well developed: For $\alpha < 1/2$, the highest energy eigenstate is almost exhausted by the single coherent state emerging from the odd balanced mean-field state (42); for $\alpha > 1/2$, the highest pair of states is exhausted by the pair (52) made up from linear combinations of two unbalanced coherent states. When the particle number is increased to $N = 100$, this crossover already becomes remarkably sharp, as witnessed by Figure 5.

On the mean-field level, a dynamical consequence of the emergence of unbalanced stationary states is a "self-trapping transition" that affects the coherent population oscillations between both wells [5,6,8]; an analogous effect had been found by Kenkre and Campbell when studying the motion of a polaron on a dimer [10]. Namely, if initially all particles are trapped in one of the two wells, quantum mean-field tunnelling leads to perfect, time-periodic

exchange of population between both wells as long as $|\alpha| < 1$, whereas the atoms become self-trapped, so that the exchange of population is imperfect, when $|\alpha| > 1$. More precisely, if one takes the population imbalance (21) initially as $p(0) = 1$, one finds

$$p(\tau) = \begin{cases} \mathrm{cn}(\tau\,, |\alpha|) & \text{for } |\alpha| < 1 \\ \mathrm{sech}(\tau) & \text{for } |\alpha| = 1 \\ \mathrm{dn}(\alpha\tau\,, 1/|\alpha|) & \text{for } |\alpha| > 1 \end{cases}, \tag{54}$$

where $\mathrm{cn}(z,k)$ and $\mathrm{dn}(z,k)$ are Jacobian elliptic functions [24,25]; this solution (54) is adapted from the Kenkre-Campbell solution [10] to the present case, and discussed in some detail, in Appendix A. Note that $\mathrm{cn}(z,k)$ oscillates cosine-like between $+1$ and -1, whereas $\mathrm{dn}(z,q)$ oscillates merely between $+1$ and $+\sqrt{1-q^2}$; the periods of oscillation are

$$T = \begin{cases} 4K(|\alpha|) & \text{for } |\alpha| < 1 \\ \frac{2}{|\alpha|}K(1/|\alpha|) & \text{for } |\alpha| > 1 \end{cases}, \tag{55}$$

with $K(k)$ denoting a complete elliptic integral of the first kind. The imperfect dn-oscillations indicate self-trapping: When $p(0) = 0$ and $|\alpha| > 1$, the population imbalance never gets below $p(T/2) = \sqrt{1 - 1/|\alpha|^2}$. Observe also that $\mathrm{cn}(z,1) = \mathrm{dn}(z,1) = \mathrm{sech}(z)$, so that $p(\tau)$ depends continuously on $|\alpha|$.

The question now is how accurate the mean-field approximation (54) describes the evolution of the actual N-particle system. Figure 6 shows the exact dynamics for $\alpha = 0.5$ and $N = 100$: Initially, at $\tau = 0$, all particles were concentrated in the first well,

$$|\Psi(\tau = 0)\rangle = |\vartheta = 0, \varphi = 0\rangle = |n_1 = N, n_2 = 0\rangle, \tag{56}$$

the time-dependent Schrödinger equation for $|\Psi(\tau)\rangle$ has been solved numerically, and the expectation values $\langle J_{x,z}\rangle/N \equiv \langle\Psi(\tau)|J_{x,z}|\Psi(\tau)\rangle/N$ have been plotted; note that $\langle J_z\rangle/N$ is the N-particle-analogue of the mean-field imbalance $p(\tau)/2$. Unlike the perfect mean-field oscillation (54), the exact 100-particle oscillation $\langle J_z\rangle/N$ shows a rapid collapse towards an equilibrated distribution within less than 10 periods, followed by a partial revival between $\tau \approx 500$ and $\tau \approx 750$. Such collapses and revivals are necessary consequences of the discreteness of the N-particle system's energy spectrum [5,26,27], with the characteristic time scales depending markedly on N: Figure 7 depicts the dynamics for $N = 1000$, again with $\alpha = 0.5$. Now the initial collapse takes longer, but there is no significant revival up to $\tau = 1000$. It should be kept in mind that the N-particle Hamiltonian contains no dissipation, so that the apparent "damping" observed in Figure 7 still results from perfectly coherent time evolution. Coming back to the estimates made in Section 2, an interval $\Delta\tau = 1000$ corresponds to $\Delta t \approx 45$ s when $\Omega = 22\ \mathrm{s}^{-1}$, so that the 1000-particle oscillation decays within no more than 5 seconds. In a laboratory experiment, of course, some real dissipation would be present. If the characteristic time scale for the loss of coherence were significantly longer than the time of a coherent collapse – say, about 10 seconds in the present example – it might actually become feasible to observe this intrinsic "coherent damping" of the N-particle oscillation, with dissipation merely destroying the long-time revivals.

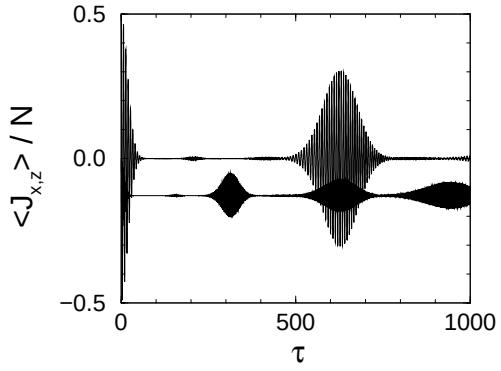

Fig. 6. N-particle population imbalance $\langle J_z\rangle/N$ (upper curve), and expectation value $\langle J_x\rangle/N$, for $N = 100$ Bose particles, and $N\kappa/\Omega = 0.5$. The initial state at $\tau = 0$ was given by the Fock state (56), expressing confinement of all particles to one well.

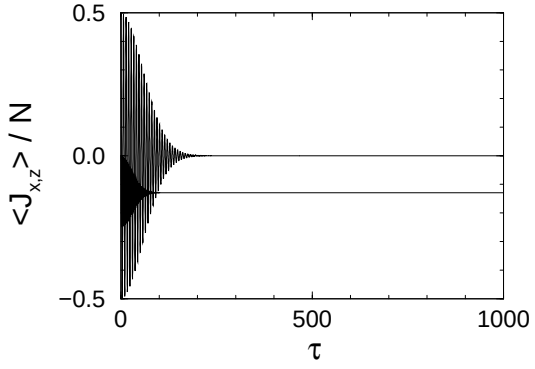

Fig. 7. As Figure 6, but with $N = 1000$ particles. The interaction strength has been reduced such that, again, $N\kappa/\Omega = 0.5$. Note that even up to $\tau = 1000$ there is no significant revival following the initial collapse. This apparent "damping" of the N-particle oscillation results from perfectly coherent dynamics.

Although it misses collapses and revivals, the approximation (54) works quite well for short times. Figure 8 compares the exact N-particle imbalance $\langle J_z\rangle/N$, again for $\alpha = 0.5$ and both $N = 100$ and $N = 1000$, with the mean-field prediction $p(\tau)/2 = \mathrm{cn}(\tau,\, \alpha)/2$. Evidently, the oscillation period does not depend on the particle number, and the mean-field picture captures this period very accurately.

The mean-field approximation becomes valid even for very long times when N is made very large, while $\alpha = N\kappa/\Omega$ is kept constant [5,18,28]. However, this limit is hard to attain in practice, if one aims at exploring

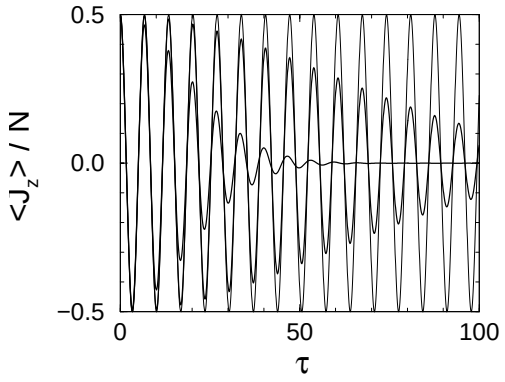

Fig. 8. Comparison of the exact N-particle imbalance $\langle J_z\rangle/N$, for $N\kappa/\Omega = 0.5$ and both $N = 100$ (heavy line, rapidly damped) and $N = 1000$ (heavy line, slowly damped), with the mean-field approximation (54) (thin line). Observe that this approximation accurately captures the exact oscillation period.

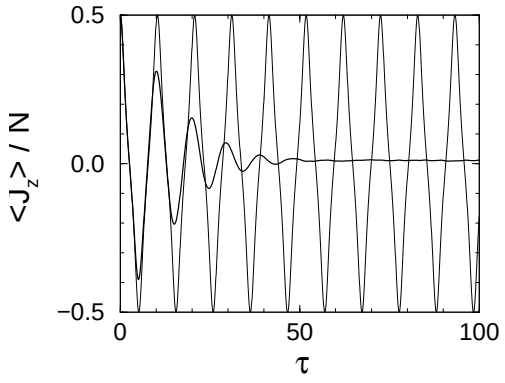

Fig. 9. Exact N-particle imbalance $\langle J_z\rangle/N$ for $N = 1000$ and $N\kappa/\Omega = 0.95$ (heavy line), compared to the mean-field approximation (54) (thin line). The initial state for the 1000-particle computation was the Fock state (56).

the interesting regime $|\alpha| \approx 1$. Namely, combining equations (15) and (17) yields

$$\frac{\kappa}{\Omega} = \frac{1}{2^{3/2}}\,\frac{a_{\rm sc}}{d}\,\exp\left(+\frac{d^2}{2\ell^2}\right), \tag{57}$$

which leaves comparatively little freedom: For establishing a weak tunnelling link, the well-to-well separation $2d$ should exceed the combined oscillator length 2ℓ of the two on-site orbitals, so that the exponential in equation (57) is at least on the order of unity. Then κ/Ω is mainly fixed by the ratio $a_{\rm sc}/d$ of the scattering length to the half-distance between the wells. With $a_{\rm sc}$ on the order of a few nm, and d on the order of a few μm, one typically has κ/Ω on the order of 10^{-3}.

Hence, it is of interest to explore what remains of the mean-field self-trapping transition for double-well potentials containing about 1000 particles; the previous Figures 4 and 5, indicating that the appearance of "unbalanced" stationary states indeed makes itself felt even in such small systems, gives rise to some optimism. Figure 9 compares the 1000-particle imbalance $\langle J_z\rangle/N$ for $\alpha = 0.95$, again computed with the Fock state (56) as initial state, to the mean-field result (54). Now the damping is more rapid than previously for $\alpha = 0.5$; the closeness to the transition point reflects itself in the fact that the oscillation does no longer equilibrate exactly to zero. When α is increased to 0.99 (Fig. 10), the exact dynamics deviate from the mean-field oscillation after even shorter time, and the long-time average of the exact imbalance increases slightly; a tendency which is continued for $\alpha = 1.01$, barely above the critical value (Fig. 11). Farther away from this critical value, for $\alpha = 1.05$, the mean-field picture becomes better again (Fig. 12); well above that value, for $\alpha = 1.50$, the mean-field approximation describes at least the first few oscillations correctly (Fig. 13). Now the exact 1000-particle oscillation levels off to the average of the imperfect dn-oscillation,

$$\langle J_z\rangle/N \to \left(1 + \sqrt{1 - 1/|\alpha|^2}\right)/4. \tag{58}$$

To summarize, while there is no sharp self-trapping transition for double wells containing a few thousand particles,

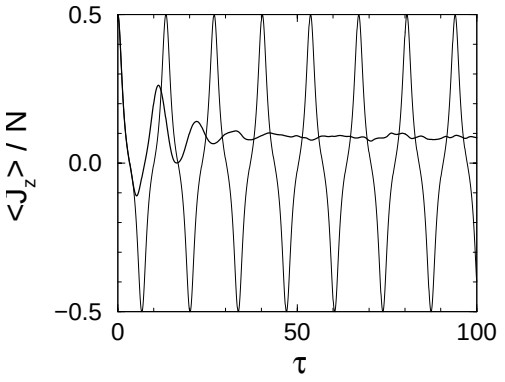

Fig. 10. As Figure 9, but with $N\kappa/\Omega = 0.99$.

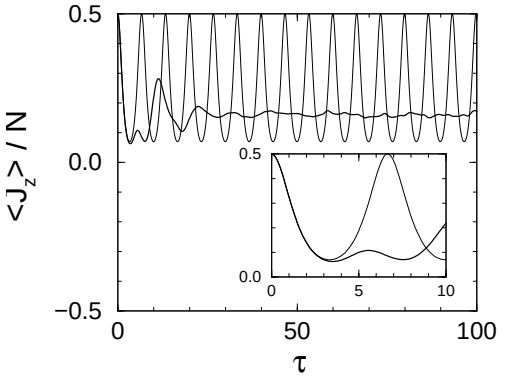

Fig. 11. As Figure 9, but with $N\kappa/\Omega = 1.01$. The previous perfect cn-type mean-field oscillations have given way to the imperfect dn-type oscillations. The inset shows that the validity of the mean-field approximation is restricted to the first half-period.

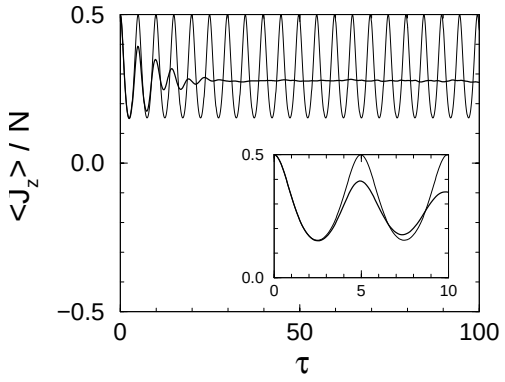

Fig. 12. As Figure 9, but with $N\kappa/\Omega = 1.05$.

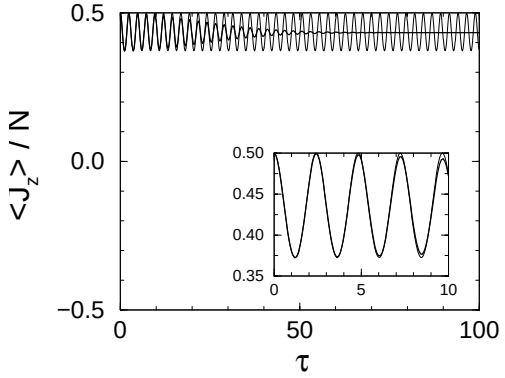

Fig. 13. As Figure 9, but with $N\kappa/\Omega = 1.50$. Observe that the exact N-particle oscillation accurately levels off to the average of the mean-field dn-oscillation, as described by equation (58).

and while the mean-field oscillations persist only for a few periods in the transition regime, the very essence of self-trapping remains intact: For $|\alpha| > 1$, the atoms tend to remain trapped in the initially populated well, such that the averaged population imbalance is given by equation (58) when $|\alpha|$ is sufficiently large. Because a self-trapped, unbalanced state involves odd or even linear combinations of almost degenerate energy eigenstates, as shown in Figures 2 and 3, self-trapping cannot be sustained indefinitely on the N-particle level, but well-to well tunnelling still occurs on the long time scale determined by the energy differences within the degenerate pairs. However, in typical short-time experiments this slow tunnelling process would go undetected.

4 The response to a periodic force

A convenient tool for visualizing, on the mean-field level, the effect of the periodic force on the coupled Bose-Einstein condensates is furnished by the nonrigid-pendulum representation (23). Taking an arbitrary point (φ_0, p_0) in the φ-p–plane as initial condition, solving the equations of motion and recording the resulting points $(\varphi(nT), p(nT))$ once every period $T = 2\pi(\omega/\Omega)^{-1}$ of the

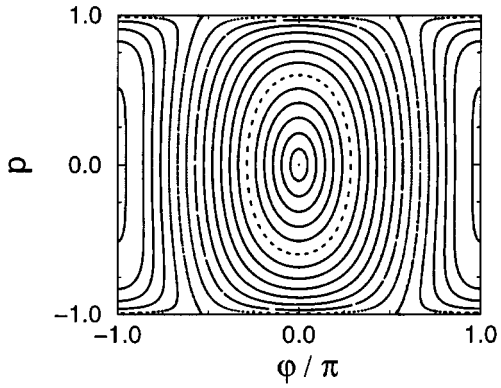

Fig. 14. Poincaré surface of section for the nonrigid pendulum (23) with $N\kappa/\Omega = 0.5$ in the absence of the force, for $\mu/\Omega = 0$. The elliptic fixed point $(\varphi = 0, p = 0)$ in the center of the plot corresponds to the stationary mean-field state (42) with the "plus"-sign. The other fixed point $(\varphi = \pi, p = 0)$, corresponding to the stationary state (42) with the "minus"-sign, is on the verge of bifurcation, giving birth to the the unbalanced mean field states (47).

drive (*i.e.*, for $n = 0, 1, 2, 3, \ldots$), then varying the initial condition and repeating this procedure, one obtains a stroboscopic picture of the dynamics, the so-called Poincaré map [23]. Figure 14 depicts a plot of such a Poincaré map for $N\kappa/\Omega = 0.5$, still for vanishing driving amplitude, $\mu/\Omega = 0$. This plot features two fixed points, one in the center $(\varphi = 0, p = 0)$, one at the edge, $(\varphi = \pi, p = 0)$ (note that the edges $\varphi = -\pi$ and $\varphi = +\pi$ have to be identified). Obviously, these fixed points correspond directly to the stationary mean-field states: the one in the center to the state (42) with the "plus"-sign, the one at the edge to the state (42) with the "minus"-sign; the fact that these two stationary states are population-balanced is immediately visible since they fall on the line $p = 0$. While the "elliptic" fixed point in the center is linearly stable, in accordance with the analysis in Section 3, the fixed point at the edge is just on the verge of bifurcation, giving birth to the unbalanced mean-field state (47) and its population-swapped counterpart.

The picture changes drastically when the periodic drive is turned on. Figure 15 shows a Poincaré plot with $N\kappa/\Omega = 0.5$ as before, but now for $\mu/\Omega = 0.3$ and $\omega/\Omega = 1.0$, so that the driving frequency precisely matches the single-particle tunnelling frequency (6). Most of the previous invariant curves have been destroyed and replaced by a seemingly irregular pattern of points, indicating that the driven mean-field dynamics are chaotic. However, embedded in this chaotic sea there still are three islands of (predominantly) regular motion, with a stable fixed point in the center of each. As in the undriven case, these fixed points have special significance. In terms of the mean-field amplitudes considered in the system (12), a fixed point of the Poincaré map corresponds to a solution $c_{\rm fp}(\tau) \equiv (c_1(\tau), c_2(\tau))$ which reproduces itself up to

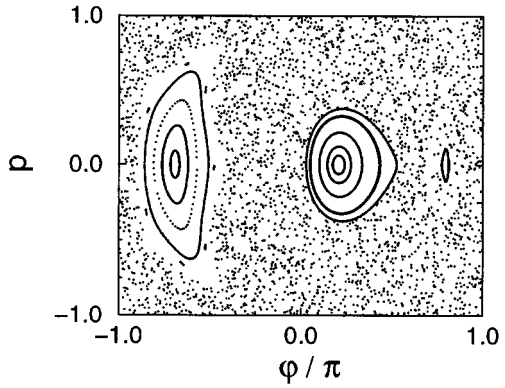

Fig. 15. Poincaré surface of section for the nonrigid pendulum (23) with $N\kappa/\Omega = 0.5$ under the influence of a time-periodic force with amplitude $\mu/\Omega = 0.3$ and frequency $\omega/\Omega = 1.0$, showing that the driven mean-field dynamics are chaotic. The fixed point in the center of each of the three regular islands corresponds to a balanced nonlinear Floquet state.

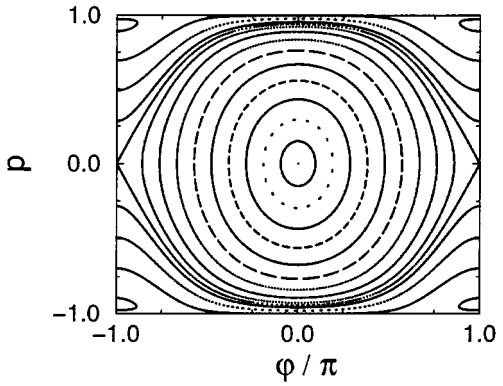

Fig. 16. Poincaré surface of section for higher interaction strength, $N\kappa/\Omega = 1.5$, and vanishing force, $\mu/\Omega = 0$. Besides the stable fixed point $(\varphi = 0, p = 0)$ and the unstable fixed point $(\varphi = \pi, p = 0)$, there are two further stable fixed points in the lobes at the edges, corresponding to the unbalanced mean-field state (47) and its population-swapped counterpart.

an overall phase factor after every period T of the force,

$$c_{\rm fp}(\tau + T) = c_{\rm fp}(\tau)\, {\rm e}^{{\rm i}\gamma_{\rm fp}}. \tag{59}$$

Writing, in analogy to the stationary states (38) in the absence of the drive, that phase factor as $\exp({\rm i}\gamma_{\rm fp}) = \exp(-{\rm i}\nu_{\rm fp}T)$, the fixed-point solutions take the form

$$c_{\rm fp}(\tau) = u_{\rm fp}(\tau)\, \exp(-{\rm i}\nu_{\rm fp}\tau), \tag{60}$$

where the functions $u_{\rm fp}(\tau)$ defined by this equation inherit the temporal periodicity of the driving force,

$$u_{\rm fp}(\tau) = u_{\rm fp}(\tau + T). \tag{61}$$

This representation (60) makes it clear that the fixed-point solutions to the system (12) are nothing but generalizations of the Floquet states known from periodically driven quantum systems to the present mean-field system obeying a nonlinear Gross-Pitaevskii equation. Briefly, the time-dependent Schrödinger equation ${\rm i}\hbar\,\partial_t|\psi(t)\rangle = H(t)\,|\psi(t)\rangle$ for a system governed by a periodically time-dependent Hamiltonian $H(t) = H(t+T)$ admits solutions of the form [12,13]

$$|\psi_n(t)\rangle = |u_n(t)\rangle\, \exp(-{\rm i}\varepsilon_n t/\hbar)\,, \tag{62}$$

with T-periodic Floquet functions

$$|u_n(t)\rangle = |u_n(t+T)\rangle \tag{63}$$

and "quasienergies" ε_n. While the formal similarity of these linear Floquet states to their nonlinear analogues (60) is obvious, there still are a number of conceptual differences. For instance, the Floquet index $\nu_{\rm fp}$ should not be regarded as a quasienergy, but rather as a frequency, since, in contrast to the Schrödinger case, the mean-field relation between energy and frequency is nonlinear (*cf.* Eq. (43) *vs.* Eq. (44), and the corresponding relations for the unbalanced states). Moreover, a periodically forced L-level system possesses precisely L Schrödinger Floquet states, whereas the number of nonlinear Floquet states is a priori uncertain, since these latter states are subject to bifurcations. We conclude from these deliberations that (i) Floquet-type solutions to the Gross-Pitaevskii equation (12) describing periodically forced, coupled Bose-Einstein condensates exist, and that (ii) these "nonlinear" Floquet states take over the role which had been played in the absence of the force by the stationary mean-field states.

The nonlinear Floquet states now enable us to discuss the periodically driven system in close analogy to the undriven one. The Floquet states corresponding to the fixed points in the centers of the regular islands in Figure 15 are all of the balanced type, since they again fall on the line $p = 0$. (Note that this statement is made possible by the circumstance that we have chosen the moments of stroboscopic sampling as $\tau_n = n\,2\pi(\omega/\Omega)^{-1}$, when the instantaneous force vanishes.) However, for higher interaction strength one also expects unbalanced Floquet states, generalizing the previous unbalanced stationary states of the type (47). Figure 16 shows a Poincaré plot for $N\kappa/\Omega = 1.5$, well above the bifurcation, and $\mu/\Omega = 0$. There is the familiar stable fixed point in the center, the fixed point at $(\varphi = \pi, p = 0)$ now has evidently become unstable, and the lobes in the edges of the plot surround the fixed points that go with the unbalanced state (47) and its swapped counterpart. When the drive is turned on to $\mu/\Omega = 0.3$ with $\omega/\Omega = 1.0$, while keeping $N\kappa/\Omega$ at the value 1.5, one obtains Figure 17: The central fixed point still is surrounded by a large regular island; there also is a further tiny, barely visible island around $(\varphi/\pi = -0.874, p = 0)$, and there are the expected regular islands at the edges, having emerged from the lobes in the preceding Figure 16. In order to establish the distinction between "balanced" and "unbalanced" nonlinear Floquet states, Figure 18 depicts the temporal evolution of the Floquet

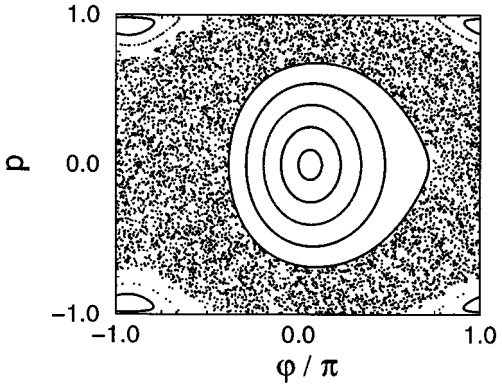

Fig. 17. Poincare surface of section for $N\kappa/\Omega = 1.5$, $\mu/\Omega = 0.3$, and $\omega/\Omega = 1.0$. The elliptic fixed points located in the islands at the corners correspond to unbalanced mean-field Floquet states. Note that there also is a tiny regular island around ($\varphi/\pi = -0.874$, $p = 0$).

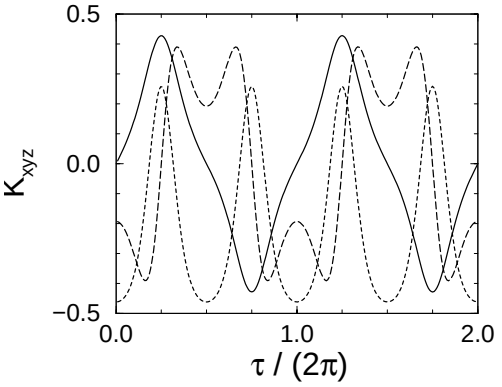

Fig. 18. Mean-field angular momentum components K_x (short dashes), K_y (long dashes), and K_z (full curve), as defined by equation (19), for the balanced nonlinear Floquet state associated with the fixed point at ($\varphi/\pi = -0.874$, $p = 0$) in Figure 17, for an interval of two periods of the driving force.

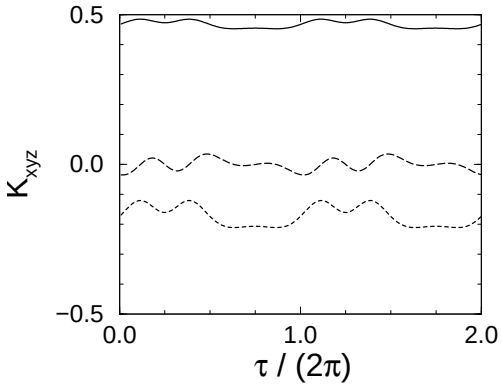

Fig. 19. As Figure 18, but now for the unbalanced mean-field Floquet state associated with the fixed point at ($\varphi/\pi = -0.938, p = 0.984$) in Figure 17.

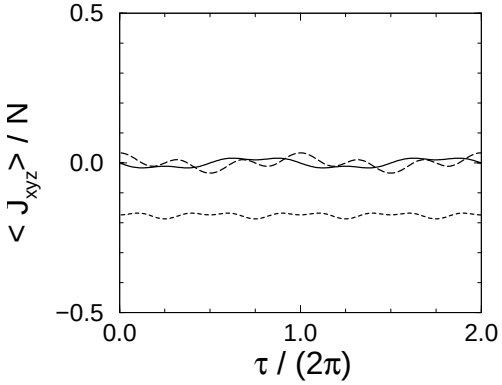

Fig. 20. N-particle expectation values of the angular momentum components J_x (short dashes), J_y (long dashes), and J_z (full line), as defined by equation (29), for an exact N-particle Floquet state with $N\kappa/\Omega = 1.5$, $\mu/\Omega = 0.3$, and $\omega/\Omega = 1.0$. This Floquet state has a partner state possessing almost the same quasienergy as itself. The number of particles is $N = 100$.

state associated with the fixed point ($\varphi/\pi = -0.874$, $p = 0$) in terms of the components K_x, K_y, and K_z of the angular momentum defined by equation (19), while Figure 19 shows the analogous plot for a Floquet state associated with one of the islands in the edges of Figure 17. The former state is manifestly balanced, with the population difference K_z oscillating symmetrically around zero, whereas the latter is strongly unbalanced, maintaining a large population surplus in the first well.

As detailed in Section 3, the exact N-particle energy eigenstates for the undriven case have definite parity and therefore are all of the balanced type. However, they come in almost degenerate pairs, so that forming odd and even superpositions of the members of such a pair gives unbalanced N-particle states which initially are concentrated in one of the wells, and remain so for rather long times, since the energy difference between the two eigenstates is almost negligible. The driven system no longer respects parity, but there is a substitute, since the Hamiltonian (28) remains invariant if parity inversion (corresponding to interchanging the indices 1 and 2) is followed by a shift in time by half a driving period. Accordingly, the exact N-particle Floquet states, which can be computed numerically by standard techniques [12], are eigenstates of this generalized parity operation. We find that, analogous to the undriven case, (i) a fraction of these Floquet states comes in pairs with almost degenerate quasienergies if $N|\kappa|/\Omega$ is sufficiently large, and that, while the individual Floquet states are population-balanced if averaged over time, (ii) one obtains unbalanced, almost T-periodic N-particle states by forming superpositions of these almost degenerate, balanced quasienergy eigenstates. An example for the evolution of an exact N-particle Floquet state, now represented by the expectation values of the components J_x, J_y, and J_z of the quantum angular momentum (29), is displayed in Figure 20. The parameters again are $N\kappa/\Omega = 1, 5$, $\mu/\Omega = 0.3$, and $\omega/\Omega = 1.0$; the particle number is $N = 100$. This state is one of the "paired" Floquet states, *i.e.*, it possesses a partner state

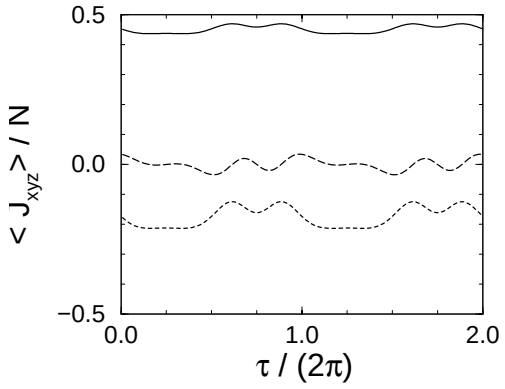

Fig. 21. As Figure 20, but now for a superposition of the Floquet state considered there with its partner state. This superposition exhibits a strong, long-lasting population imbalance. From the difference of the two quasienergies, we estimate that the population will have tunnelled to the other well only after more than 8×10^6 driving periods.

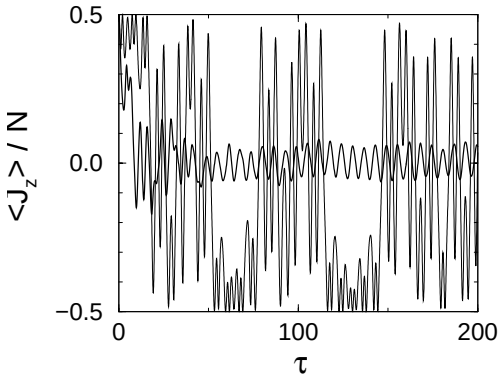

Fig. 22. Exact N-particle imbalance $\langle J_z \rangle / N$, for $N = 1000$ and $N\kappa/\Omega = 1.4$, in the presence of a periodic force with parameters $\mu/\Omega = 0.3$ and $\omega/\Omega = 1.0$ (heavy line); all particles were initially trapped in the first well. Although the scaled interaction strength is much higher than the value $N\kappa/\Omega = 1.0$ marking the onset of self-trapping in the absence of the force, the time-averaged imbalance soon tends to zero. The thin line shows the mean-field prediction for the same set of parameters.

with a quasienergy almost identical to its own. Forming a superposition of these two states, one finds the strongly unbalanced N-particle state depicted in Figure 21. From the small difference between the two quasienergies of this particular pair, we estimate that the population imbalance will be inverted by collective tunnelling to the other well only after more than 8×10^6 periods of the driving force. With $\omega = 22\ \mathrm{s}^{-1}$, as corresponding to the estimate in Section 2, this implies a tunnelling time of close to a month.

The above analogy between the undriven and the driven dynamics now leads one to expect that there also should be something akin to the self-trapping transition in the presence of the periodic drive: If initially all condensed Bose particles are stored in one of the wells, they should visit both wells equally as long as the scaled interaction strength $N|\kappa|/\Omega$ stays below a certain critical value (which, again, will not be defined sharply on the N-particle level, but rather should be regarded as a value characterizing the center of a transition regime; *cf.* the gradual transition displayed in Figs. 9 to 12), but maintain a long-lasting population imbalance when $N|\kappa|/\Omega$ is enhanced. Most importantly, that critical value of the interaction strength, now reflecting the presence of unbalanced (on the mean-field level) or paired (on the N-particle level) Floquet states, should depend on the parameters of the force, as do the Floquet states themselves, and could thus be quite different from the critical value $N|\kappa|/\Omega = 1.0$ which marks the transition in the absence of the drive. In other words, it should be possible to coherently control the onset of self-trapping by the external force. This expectation is fully borne out by the following two plots: Figure 22 shows the evolution of the population imbalance, after initially $N = 1000$ Bosons had been trapped in the first well, for $N\kappa/\Omega = 1.4$, and $\mu/\Omega = 0.3$, $\omega/\Omega = 1.0$. Although the scaled interaction strength is significantly higher here than $N|\kappa|/\Omega = 1.0$, this figure still is reminiscent of Figure 9, signalling untrapped evolution: After

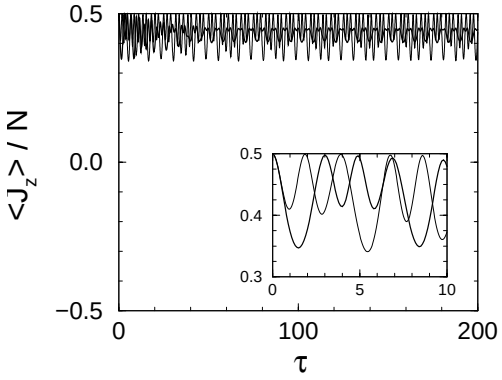

Fig. 23. As Figure 22, but now for $N\kappa/\Omega = 1.6$. The parameters of the periodic drive are the same as before. The inset shows that the exact N-particle dynamics (heavy line) follows the mean-field prediction (thin line) only for a rather short time interval.

an initial transient, the N-particle population imbalance becomes almost zero on the average; naturally, the instantaneous imbalance has to follow the driving force to some extent and therefore does not approach a constant value. Again in close analogy to Figure 9, the mean-field prediction for the same situation shows (chaotic) oscillations covering (almost) the entire range between $+0.5$ and -0.5. This changes when $N\kappa/\Omega$ is increased to 1.6: As displayed in Figure 23, which should be contrasted to the previous Figure 12, the population now actually remains trapped in the initially occupied well, both on the mean-field and on the N-particle level, although the mean-field picture differs in detail strongly from the exact N-particle evolution already for $\tau \geq 1$. Of course, on the N-particle level, on a long time scale determined by the difference between the quasienergies of the paired N-particle Floquet states, self-trapping will once more be destroyed by

tunnelling and the N Bosons will actually fill the other well; however, under typical conditions that time scale is way too long to be of experimental significance.

It should be noted that the force acting here on the Bose Josephson junction is not strong, the quantum $\hbar\omega$ just equalling the single-particle tunnelling splitting, and the energy $\hbar\mu$ associated with the driving amplitude amounting to merely 30% of that quantum. Yet, the effect of even that weak force is substantial, shifting the onset of self-trapping from $N\kappa/\Omega = 1.0$ in the absence of the drive to about 1.5, that is, by roughly 50% upward. We conclude that already a weak periodic force offers an efficient means of predetermining that value of the scaled interaction strength $N\kappa/\Omega$ where self-trapping is desired to occur. Besides the existence of Floquet-type solutions to the Gross-Pitaevskii equation, the parallels between the mean-field picture and the full N-particle evolution, and the far-reaching analogy between the undriven and the driven dynamics, this sensitivity of the mechanism for coherently controlling the self-trapping transition to the parameters of the drive is one of the main results of this work.

5 Conclusions

In the absence of the driving force, the existence of unbalanced stationary mean-field states of the type (47) – that is, of solutions to the nonlinear Schrödinger equation (40) which imply a perpetual asymmetric distribution of the condensed atoms over both wells – brings about the self-trapping transition described by equation (54): Confining initially the entire condensate to one well, complete, periodic tunnelling to the other well and back is possible only as long as the absolute value of the scaled interaction strength $\alpha = N\kappa/\Omega$ is lower than unity [5,6,8,10]. This mean-field result applies to the limit of large particle number ($N \to \infty$) and weak interaction ($\kappa \to 0$), taken such that α remains constant [28]. However, the estimate (57) indicates that under typical laboratory conditions the interesting regime $|\alpha| \approx 1$ will be reached with comparatively small condensates containing merely on the order of 10^3 atoms. The exact N-particle dynamics then exhibit collapses and revivals, thus differing strongly from the mean-field picture. Yet, in essence self-trapping still persists, albeit not for infinite times. This persistence is made possible by the gradual appearance of pairs of almost degenerate energy eigenstates which, although strictly balanced themselves, are made up from unbalanced coherent states according to the pattern (52).

When the double well is modulated periodically in time, with period T, the mean-field dynamics undergo a profound change and become chaotic. Nonetheless, there remain strong parallels to the undriven case. The role of the stationary mean-field states is taken over by the Floquet states (60), which reproduce themselves (apart from an overall phase factor) after every period of the drive, and which can again be classified as "unbalanced" or "balanced", depending on whether or not they entail permanent asymmetric atom distribution. As in the undriven case, the unbalanced states lead to a mean-field self-trapping transition; this transition survives on the N-particle level, in somewhat smoothed form, down to fairly small N. The survival is mediated by pairs of balanced N-particle Floquet states from which almost T-periodic, unbalanced wave functions can be built; the tiny difference between the quasienergies of the members of such a pair sets the time scale for the ultimate loss of self-trapping due to collective tunnelling.

The existence of Floquet-type solutions for the nonlinear Schrödinger equation (12) could be ascertained by linking these states to the fixed points of a Poincaré section in the plane of relative phase φ and population imbalance p, as in Figures 15 and 17. Without possessing a formal proof, we surmise that such nonlinear Floquet states exist also for other set-ups with forced Bose-Einstein condensates; if so, Floquet states should be of outstanding value for analyzing a whole wealth of novel effects. For instance, harmonic generation and nonlinear coupling in the dynamics of strongly driven Bose-Einstein condensates have already been observed [29]; since the Floquet states incorporate the periodic drive in a non-perturbative manner, they should be *the* tools for understanding such phenomena outside the regime of linear response.

The point of view adopted in Section 4 may be characterized as an active one: In the absence of the driving force the self-trapping transition occurs for $|\alpha| = 1$, in the presence of that force the onset of self-trapping is shifted to different values of α by suitably adjusting its strength and frequency; we have shown that even weak forces can effectuate substantial shifts. Measuring such shifts could be exploited for determining the scattering length $a_{\rm sc}$ (if N is known beforehand), or the precise number of particles (if $a_{\rm sc}$ is known). One might, however, also maintain that it is not the transition which is shifted to different α as a result of the force, but rather that the effective value of α is changed, implying that the periodic force renormalizes the interaction strength. This alternative, passive viewpoint is suggested by Figure 24, which shows the quasienergies of the exact N-particle Floquet states as functions of the driving amplitude μ/Ω, for $N = 100$, $N\kappa/\Omega = 0.7$, and the rather high frequency $\omega/\Omega = 200$. According to the estimates in Section 2, such a high frequency certainly falls outside the regime of validity of the two-mode approximation, but it allows us to avoid a complication brought about by the Brillouin zone-structure of the quasienergy spectrum: As is evident from equations (62) and (63), the separation of a Floquet state $|\psi_n(t)\rangle$ into a T-periodic function $|u_n(t)\rangle$ and a phase factor $\exp(-\mathrm{i}\varepsilon_n t/\hbar)$ is determined only up to a phase factor $\exp(-\mathrm{i}\omega t)$, with $\omega = 2\pi/T$, so that the quasienergies are defined only up to an integer multiple of $\hbar\omega$. Therefore, the quasienergy spectrum is arranged in zones of width $\hbar\omega$, each zone containing one representative of the quasienergy of each state. With $\omega/\Omega = 200$ in Figure 24, the width of the Brillouin zone there exceeds the difference of the highest and the lowest unperturbed N-particle energy eigenvalue, so that folding the levels into the fundamental zone

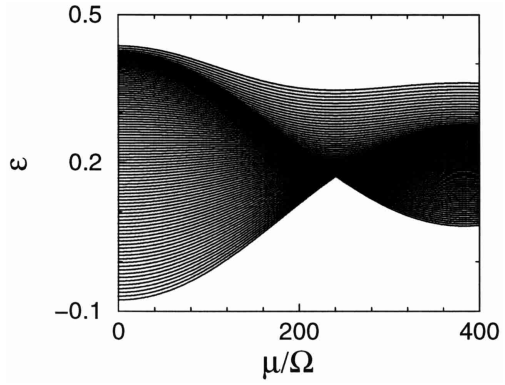

Fig. 24. Exact quasienergies ε_n (in multiples of $\hbar\omega$) for $N = 100$, $N\kappa/\Omega = 0.7$, and high frequency $\omega/\Omega = 200.0$, as functions of the driving amplitude μ/Ω. The unpaired quasienergies vary about proportional to the ordinary Bessel function $J_0(2\mu/\omega)$, leading to the focusing of these eigenvalues at $\mu/\Omega \approx 240$, when the argument $2\mu/\omega$ equals the first zero of J_0. The number of paired eigenvalues emerging above the J_0-pattern depends strongly on μ/Ω, being largest at the point of focus.

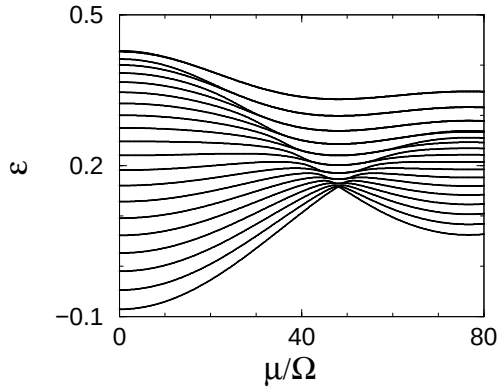

Fig. 25. As Figure 24, but now for $N = 20$. The value of $N\kappa/\Omega$ again is 0.7, while the driving frequency has been reduced by the same factor as the particle number to $\omega/\Omega = 40.0$. Pairing and unpairing of quasienergies in the vicinity of the focus point at $\mu/\Omega \approx 48$, where $2\mu/\omega$ equals the first zero of the Bessel function J_0, are clearly visible here.

does not change their relative position. (Had we chosen the realistic frequency $\omega/\Omega = 1.0$ instead, as in the case study in Sect. 4, projecting the levels into a single zone would have resulted in a multitude of near-degeneracies – avoided crossings – which reflect the chaotic mean-field dynamics, but would only unnecessarily complicate matters here.) For $\mu/\Omega = 0$, at the left margin, Figure 24 leads us back to Figure 2 with $N\kappa/\Omega = 0.7$: Most of the eigenvalues are unpaired; only at the high end of the spectrum a few paired quasienergies emerge, belonging to interaction-dominated states. When μ/Ω is increased, the unpaired eigenvalues in Figure 24 appear to get focused, such that the distance between the highest and lowest unpaired quasienergy decreases proportional to $J_0(2\mu/\omega)$, where $J_0(z)$ denotes the zero-order Bessel function; when $\mu/\Omega \approx 240$, so that the argument $2\mu/\omega$ reaches the first zero $j_{0,1} \approx 2.405$ of J_0, the unpaired quasienergies collapse to a single value. This J_0-pattern is well known in the theory of periodically forced quantum systems; it always occurs when a chain of entities with nearest-neighbour coupling is modulated by a time-periodic dipole-type force. Among the older examples are the J_0-proportional modification of atomic g-factors for atoms in oscillating magnetic fields [30,31], where the nearest neighbours are adjacent atomic angular momentum substates, or the J_0-proportional band narrowing for semiconductor superlattices in far-infrared laser fields [31], where the nearest neighbours are adjacent superlattice sites; traces of this band narrowing have recently been detected in experiments with cold atoms in periodically forced optical lattices [32]. The conspicuous J_0-pattern in Figure 24 constitutes another example; here the nearest neighbours are adjacent states in two-site Fock space spanned by the number states $|n_1, n_2\rangle$ (*cf.* Eq. (35)). Thus, the appearance of this J_0-pattern obeyed by the unpaired states was to be expected on general grounds. What could not be expected, though, and leads to the passive viewpoint we are aiming at, is the emergence of more and more paired quasienengies on top of the focusing unpaired eigenvalues when $2\mu/\omega$ approaches $j_{0,1}$ from below, and the re-transformation of paired states into unpaired ones when the amplitude is increased beyond the focus point. This gradual pairing and unpairing of quasienergies for scaled driving amplitudes $2\mu/\omega$ in the vicinity of $j_{0,1}$ is particularly obvious in Figure 25, where the number of particles has been reduced to $N = 20$, and the frequency has been adjusted accordingly. Comparing the N-particle quasienergies displayed in these two Figures 24 and 25 to the energy eigenvalues shown in Figures 2 and 3, we conclude that varying the driving amplitude has a similar effect as varying the scaled interaction strength, insofar as both parameters effectively control the ratio of the number of interaction-dominated, paired to that of unpaired states; increasing μ/Ω in Figure 24 beyond the focus point is tantamount to first increasing and then decreasing $N\kappa/\Omega$ in Figure 2. This is what ultimately provides the mechanism for coherently controlling the self-trapping transition, and this is the basis of our passive interpretation: Modulating the double-well amounts to renormalizing the strength of the interaction among the condensed atoms. Whether this renormalization is a specific feature of Bose-Einstein condensates in periodically modulated double-well potentials, or whether is also occurs under different conditions, is an open question.

M.H. thanks Professor Herbert Wagner for kind hospitality at the Ludwig-Maximilians-Universität München, where part of this work was done. He also gratefully acknowledges support through a Heisenberg fellowship from the Deutsche Forschungsgemeinschaft.

Appendix A: Evolution of population imbalance within the mean-field approximation

A convenient starting point for deriving the mean-field dynamics of the population imbalance $p(\tau)$ for $\mu/\Omega = 0$ [8,10] is the nonrigid-pendulum Hamiltonian (24),

$$H_{\rm nrp} = \alpha p^2 - \sqrt{1-p^2}\cos(\varphi), \tag{A.1}$$

together with the equation of motion

$$\dot{p} = -\sqrt{1-p^2}\sin(\varphi). \tag{A.2}$$

We fix $H_{\rm nrp} \equiv \eta$, so that, by construction, the constant of motion η denotes the energy per particle in multiples of the tunnelling splitting,

$$\eta = \frac{E/N}{\hbar\Omega}\cdot \tag{A.3}$$

A brief calculation furnishes the bounds on η,

$$\begin{aligned} -1 \le \eta \le +1 \quad &\text{for} \quad |\alpha| \le 1/2 \\ -4|\alpha| \le 4\alpha\eta \le 4\alpha^2+1 \quad &\text{for} \quad |\alpha| \ge 1/2; \end{aligned} \tag{A.4}$$

recall that positive α correspond to repulsive and negative α to attractive interactions among the condensed atoms. Squaring and adding equations (A.1) and (A.2) then yields

$$\dot{p}^2 + \left(\alpha p^2 - \eta\right)^2 = 1 - p^2, \tag{A.5}$$

or

$$\dot{p} = \pm\alpha\left[(p_+^2 - p^2)(p^2 - p_-^2)\right]^{1/2}, \tag{A.6}$$

where

$$p_\pm^2 = \frac{1}{2\alpha^2}\left[2\alpha\eta - 1 \pm \sqrt{4\alpha^2+1-4\alpha\eta}\right]. \tag{A.7}$$

Using the inequalities (A.4), one easily shows that in any case both p_-^2 and p_+^2 are real numbers, and that p_+^2 is always non-negative. In contrast, p_-^2 changes its sign when $|\eta| = 1$ (more precisely, for $\alpha > 0$ the change of sign occurs when $\eta = 1$; for $\alpha < 0$ when $\eta = -1$). This necessitates distinguishing two cases:

(i) When $|\eta| < 1$, one has $p_-^2 < 0$. Casting then equation (A.6) into the form

$$\dot{p} = \pm\alpha\,\frac{p_+^2}{k}\left[\left(1-\left(\frac{p}{p_+}\right)^2\right)\left(k^2\left(\frac{p}{p_+}\right)^2 + 1 - k^2\right)\right]^{1/2}, \tag{A.8}$$

where

$$k^2 = \frac{1}{2}\left[1 + \frac{2\alpha\eta - 1}{\sqrt{4\alpha^2+1-4\alpha\eta}}\right], \tag{A.9}$$

and observing that $k^2 < 1$, one can utilize the integral representation for the inverse of the Jacobian elliptic function cn, namely [24]

$$\mathrm{cn}^{-1}(y,k) = \int_y^1 \frac{\mathrm{d}t}{\sqrt{(1-t^2)(k^2t^2+1-k^2)}}\cdot \tag{A.10}$$

This leads immediately to

$$p(\tau) = p_+\mathrm{cn}\Big(\frac{p_+}{k}\alpha\tau + \beta\,, k\Big), \tag{A.11}$$

where the phase angle β is determined by the initial condition,

$$\beta = \mp\mathrm{cn}^{-1}\left(\frac{p(0)}{p_+}\,, k\right). \tag{A.12}$$

The function $\mathrm{cn}(z,k)$ oscillates in a cosine-like manner between $+1$ and -1, with period $4\,K(k)$, where $K(k)$ denotes a complete elliptic integral of the first kind [24,25]. Therefore, for $|\eta| < 1$ one encounters perfect, periodic exchange of population between both wells, with period

$$T = \frac{4k\,K(k)}{p_+|\alpha|}\cdot \tag{A.13}$$

(ii) When $|\eta| > 1$, one has $p_-^2 > 0$. Accordingly, rewriting equation (A.6) as

$$\dot{p} = \pm\alpha\,p_+^2\left[\left(1-\left(\frac{p}{p_+}\right)^2\right)\left(\left(\frac{p}{p_+}\right)^2 - \frac{p_-^2}{p_+^2}\right)\right]^{1/2}, \tag{A.14}$$

one is led to the representation of the inverse of the elliptic function dn [24],

$$\mathrm{dn}^{-1}(y,q) = \int_y^1 \frac{\mathrm{d}t}{\sqrt{(1-t^2)(t^2+q^2-1)}}, \tag{A.15}$$

where the modulus appearing here is just the inverse of the modulus (A.9) met in the previous case,

$$q^2 = 1 - \frac{p_-^2}{p_+^2} = \frac{1}{k^2}\cdot \tag{A.16}$$

Therefore,

$$p(\tau) = p_+\mathrm{dn}(p_+\alpha\tau + \beta\,, 1/k) \tag{A.17}$$

with

$$\beta = \mp\mathrm{dn}^{-1}\left(\frac{p(0)}{p_+}\,, \frac{1}{k}\right). \tag{A.18}$$

In contrast to $\mathrm{cn}(z,k)$, the function $\mathrm{dn}(z,q)$ oscillates merely between $+1$ and $+\sqrt{1-q^2}$, with period $2\,K(q)$. Thus, for $|\eta| > 1$ the oscillations of the population between the two wells have the period

$$T = \frac{2\,K(1/k)}{p_+|\alpha|}, \tag{A.19}$$

but these oscillations are imperfect; the atoms tend to remain trapped in the well containing the majority of them at $\tau = 0$.

Since the value of η is determined by the initial condition (p_0, φ_0), so is the critical value of the coupling strength α where the cn-type solutions (A.11) change into the trapped dn-solutions (A.17) [8]:

$$\alpha_{\rm c} = \frac{\pm 1 + \sqrt{1 - p_0^2}\cos(\varphi_0)}{p_0^2}, \qquad \text{(A.20)}$$

implying $\alpha_{\rm c} = \pm 1$ if $p_0^2 = 1$. Since, moreover, $\mathrm{cn}(z, 1) = \mathrm{dn}(z, 1) = \mathrm{sech}(z)$, this transition occurs in a continuous manner.

The above expressions for $p(\tau)$ become particularly simple when initially all atoms are confined to one of the wells. Choosing $p_0 = 1$, the Hamiltonian (A.1) yields $\eta = \alpha$, so that equations (A.7) and (A.9) give $p_+^2 = 1$ and $k^2 = \alpha^2$, respectively. Using this, one immediately finds the results stated in equations (54) and (55).

References

1. For a review see W. Ketterle, D.S. Durfee, D.M. Stamper-Kurn, in *Proceedings of the International School of Physics "Enrico Fermi", Course CXL*; edited by M. Inguscio, S. Stringari, C.E. Wieman (IOS Press, Amsterdam, 1999).
2. J. Javanainen, Phys. Rev. Lett. **57**, 3164 (1986).
3. S. Grossmann, M. Holthaus, Z. Naturforsch. A **50**, 323 (1995).
4. M.R. Andrews, C.G. Townsend, H.-J. Miesner, D.S. Durfee, D.M. Kurn, W. Ketterle, Science **275**, 637 (1997).
5. G.J. Milburn, J. Corney, E.M. Wright, D.F. Walls, Phys. Rev. A **55**, 4318 (1997).
6. A. Smerzi, S. Fantoni, S. Giovanazzi, S.R. Shenoy, Phys. Rev. Lett. **79**, 4950 (1997).
7. I. Zapata, F. Sols, A.J. Leggett, Phys. Rev. A **57**, R28 (1998).
8. S. Raghavan, A. Smerzi, S. Fantoni, S.R. Shenoy, Phys. Rev. A **59**, 620 (1999).
9. F.Kh. Abdullaev, R.A. Kraenkel, Phys. Rev. A **62**, 023613 (2000).
10. V.M. Kenkre, D.K. Campbell, Phys. Rev. B **34**, 4959 (1986).
11. M. Holthaus, preprint (Carl von Ossietzky Universität Oldenburg, 2000).
12. J.H. Shirley, Phys. Rev. **138**, B 979 (1965).
13. Ya.B. Zel'dovich, Zh. Eksp. Theor. Fiz. **51**, 1492 (1966) [Sov. Phys. JETP **24**, 1006 (1967)].
14. R.W. Spekkens, J.E. Sipe, Phys. Rev. A **59**, 3868 (1999).
15. L.D. Landau, E.M. Lifshitz, *Quantum Mechanics* (Butterworth-Heinemann, Oxford, 1997), Chap. 50.
16. C. Herring, Rev. Mod. Phys. **34**, 631 (1962).
17. E. Tiesinga, C.J. Williams, P.S. Julienne, K.M. Jones, P.D. Lett, W.D. Phillips, J. Res. Natl. Inst. Stand. Technol. **101**, 505 (1996).
18. S. Raghavan, A. Smerzi, V.M. Kenkre, Phys. Rev. A **60**, R1787 (1999).
19. J.M. Radcliffe, J. Phys. A **4**, 313 (1971).
20. F.T. Arecchi, E. Courtens, R. Gilmore, H. Thomas, Phys. Rev. A **6**, 2211 (1972).
21. J.C. Eilbeck, P.S. Lomdahl, A.C. Scott, Physica D **16**, 318 (1985).
22. C.A. Sackett, J.M. Gerton, M. Welling, R.G. Hulet, Phys. Rev. Lett. **82**, 876 (1999).
23. J. Guckenheimer, P. Holmes, *Nonlinear Oscillations, Dynamical Systems, and Bifurcations of Vector Fields* (Springer Verlag, New York, 1990).
24. P.M. Morse, H. Feshbach, *Methods of Theoretical Physics* (McGraw-Hill, New York, 1953), pp. 427–433.
25. L.M. Milne-Thomson, *Jacobian Elliptic Functions and Theta Functions*, in *Handbook of Mathematical Functions*, edited by M. Abramowitz, I.A. Stegun (Dover, New York, 1972).
26. E.M. Wright, D.F. Walls, J.C. Garrison, Phys. Rev. Lett. **77**, 2158 (1996).
27. A. Imamoḡlu, M. Lewenstein, L. You, Phys. Rev. Lett. **78**, 2511 (1997).
28. E.H. Lieb, R. Seiringer, J. Yngvason, Phys. Rev. A **61**, 043602 (2000).
29. G. Hechenblaikner, O.M. Maragò, E. Hodby, J. Arlt, S. Hopkins, C.J. Foot, Phys. Rev. Lett. **85**, 692 (2000).
30. S. Haroche, C. Cohen-Tannoudji, C. Audoin, J.P. Schermann, Phys. Rev. Lett. **24**, 861 (1970).
31. For a review see M. Holthaus, in *Coherent Control in Atoms, Molecules, and Semiconductors*, edited by W. Pötz, W.A. Schroeder (Kluwer, Dordrecht, 1999).
32. K.W. Madison, M.C. Fischer, R.B. Diener, Qian Niu, M.G. Raizen, Phys. Rev. Lett. **81**, 5093 (1998).